Interaction of turbulent kinetic energy and coherent motion in the near field of the cylinder wake

Majd Armaly, Emilien Varea, Corine Lacour, Luminita Danaila, Bertrand Lecordier

Mechanics & Industry **24**, 44 (2023)
© M. Armaly et al., Published by EDP Sciences, 2023
https://doi.org/10.1051/meca/2023038

Mechanics & Industry

Available online at:
www.mechanics-industry.org

High fidelity models for control and optimization
Nicolas Moës and Emmanuel Guilmineau (Guest Editors)

REGULAR ARTICLE

OPEN ACCESS

Interaction of turbulent kinetic energy and coherent motion in the near field of the cylinder wake

Majd Armaly[1], Emilien Varea[1], Corine Lacour[1], Luminita Danaila[2], and Bertrand Lecordier[1,*]

[1] CORIA UMR 6614, University of Rouen Normandy, INSA of Rouen, CNRS, Saint Étienne du Rouvray, 76800, France
[2] M2C UMR 6143, University of Rouen Normandy, Mont-Saint-Aignan, 76821, France

Received: 27 February 2023 / Accepted: 26 October 2023

Abstract. The far aim of the study is to experimentally assess the exchange of turbulent kinetic energy (TKE) of a wake behind a cylinder, as a function of the upstream flow. The wake behind the obstacle is composed of coherent motion (CM) and random motion (RM). Coherent motion, reminiscent of the Von Kármán street, interacts with the random flow, thus inducing locally enhanced turbulent cascade. This energy exchange between CM and RM is reflected by the kinetic energy budget at one point, and two points in space. In the experimental setup, a cylinder is placed in a closed loop wind tunnel to create a Von Kármán vortex street. The Reynolds number, based on the cylinder diameter and the free main stream velocity, is equal to Re = 2000. Two-dimensional, two-components in-plane velocity fields are measured behind the cylinder by Particle Image Velocimetry (PIV). Two sets of measurements are explored: without and with synchronization, based on the CM. For synchronization, a microphone is used. CM is reconstructed, by filtering the flow at 9 phase shifts, for a detailed insight.

Keywords: Turbulence / wakes / triple decomposition / energy budgets for turbulent kinetic energy

1 Introduction

Wakes are widely observed on our planet, in both environmental and industrial flows, as a result of the presence of solid bodies in fluids. Flow over bluff bodies have been studied for decades. When a fluid flow passes over an obstacle, staggered vortices are created downstream. This is called Bénard–Von Kármán street, studied by e.g. Bloor [1], Roshko [2] and Williamson [3]. Unal & Rockwell [4], Abernathy & Kronauer [5] and Triantafyllou & Chryssostomidis [6] assessed the formation of the Von-Kármán street in the context of the absolute instabilities of shear layers. At higher Reynolds numbers, turbulent flows behind cylinders exhibit a wide range of scales, with different amounts of energy. The classical postulates of turbulence are based upon the concept of the cascade, i.e. kinetic energy is injected at the largest scales of the flow and is transferred to smaller scales through the cascade process. Cantwell & Coles [7] showed that a substantial fraction of the turbulent kinetic energy is primarily produced at intermediate scales near saddle points, and is later transported towards larger scales. The assessment of the energy budget in the near-wake region of a cylinder allows to detect the basic mechanisms of production, transport and dissipation of kinetic energy. Townsend [8] illustrated the turbulent kinetic energy budget for different shear flows. Instability of the shear layer is associated with production and transport of kinetic energy, whilst in other regions of the flow all processes are present. The experimental study of Thiesset [9] assessed the turbulent kinetic energy budget in the cylinder wake. Measurements were based on hot wire anemometry, which is time-resolved but focuses on a single space point. Moreover, all phases of vortex shedding are mixed together, and a careful selection of each phase was required in order to discern processes at each specific phase. The present contribution resolves this shortcoming by the use of high-fidelity optical diagnostics that offers a wider view of the flow. Moreover, measurements are performed at each particular phase of the coherent motion (CM) (any particular time in its period is usually called phase), which further simplifies the analysis. In this contribution, we focus on assessing the dynamical behavior of a wake behind a cylinder as a function of the upstream flow, at low Reynolds number ($Re \equiv \frac{DU}{\nu} = 2000$), where D is the diameter of the cylinder, ν is the kinematic viscosity, U is the free stream velocity. The Strouhal number $St \equiv \frac{fD}{U} = 0.2$, and f is the shedding frequency. The Strouhal number St may depend on different parameters such as the Reynolds number, the geometry of the obstacle, the upstream turbulence level and the cylinder roughness. From the perspective of statistics, it appears at most that the operation of averaging applied to equations of motion hides from view many important features of turbulent flow. For instance, the experimental study of Thiesset [9] assessed the turbulent kinetic energy budget in the cylinder wake at all phases of vortex shedding mixed together. The present investigation resolves this shortcoming by a careful selection of each

* e-mail: Bertrand.Lecordier@coria.fr

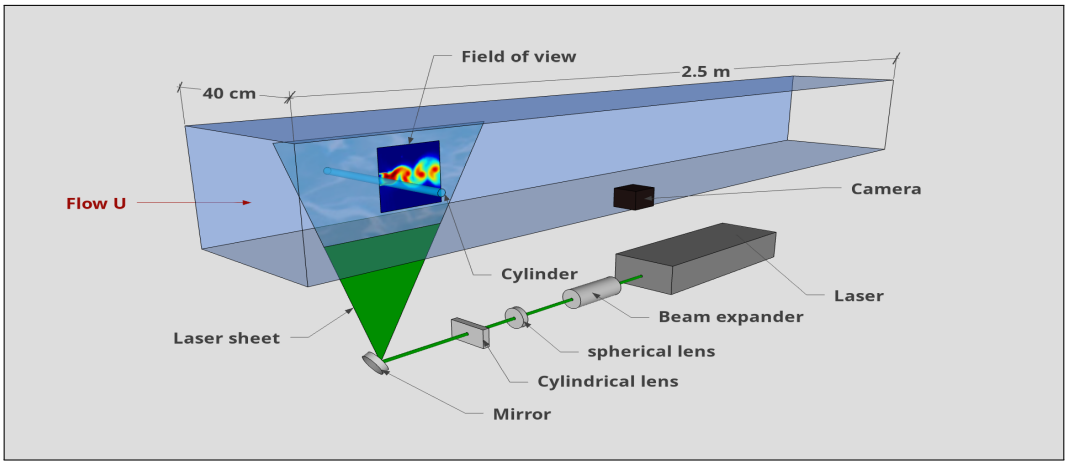

Fig. 1. Experimental setup.

phase that is required in order to discern processes at each specific phase. The paper is organized as follows:

- Experimental setup and measurements parameters.
- Triple decomposition and low order statistics (mean and RMS).
- Results pertaining to one and two points turbulent kinetic energy.
- Conclusion.

2 Experimental set-up

The experimental study is performed in a closed loop wind tunnel. The test section of the wind tunnel is a square section with dimensions of $40 \times 40\,\mathrm{cm}^2$ and 2.5 m long. The fan is located after the divergence part of the wind tunnel with a $2HP$ power and a maximum frequency of $60Hz$. The cross section is drilled at its end with an 80 mm hole to insert the smoking machine tube for particles injection. The walls of the test section allow optical diagnostics to be performed. The flow speed is set by a frequency controller which modulated the fan rotation speed. The flow velocity of the tunnel ranges from 0.23 m/s to 16.6 m/s. The upstream flow is characterized by a very low residual turbulent intensity level (smaller than 0.5%). The wake flow downstream of the obstacle is natural. It is generated by a cylinder (diameter of 10mm) with no other forcing applied.

2D-2C PIV measurements are carried out in the test section of the wind tunnel. JAI camera with a resolution of $2048 \times 2048 pixels^2$ (12 bits), working at $8fps$ are used for data acquisition. A Nd:YAG laser (532 nm) is used to illuminate $10.4 \times 10.4\,\mathrm{cm}^2$ field of view. Its maximum frequency is of 10 Hz. The laser beam passes through a beam expander, spherical lense ($f = 1000$ mm), cylindrical lense ($f = -100$ mm) and a mirror, see Figure 1. The laser sheet at the focus line is 0.5 mm thick. Time between pulses is of 20μs. The PIV post processing is performed using in-house code. The size of the interrogation window was 32×32 pixels^2 ($1.6 \times 1.6\,\mathrm{mm}^2$). Overlap is set to 50%, yielding a 127×127 vector field.

Data acquisition is synchronized with the vortex generation, thus allowing to resolve characteristic phases of the coherent motion (CM) and to eventually lead to a visualisation of the of Von Kármán vortex street. Synchronisation of data acquisition with CM generation requires first a clear detection of vortices, and of their dynamics, just behind the cylinder. Vortices detection is performed by placing a microphone sensor (Type: 4182, Sensitivity: 3.65 mv/Pa and Sampling rate: 20 kHz), after the cylinder to estimate the dynamical pressure of the flow. The microphone's position is precisely fixed after the cylinder recirculation zone ($X/D = 3.5, Y/D = 2$). The microphone is set 2–5 mm far from the measurements plane (along a direction normal to that plane) to minimize any possible influence on the flow. The microphone signal only triggers the data acquisition at the maximum pressure level. The pressure level in the flow is weak and in the frame of the acceptable range of the microphone sensibility. The pressure signal obtained from the microphone is quasi-periodic, thus indicating all phases of vortices (or, CM) generation.

Data acquisition was performed for particular phases of CM, using trigger systems as shown in Figure 2. The overlap between the pressure signal of the microphone and a synchronization signal defines the reference phase (phase = 0). The overlap leads to an acquisition signal of PIV at one particular phase of shedding vortices. Knowing the inlet velocity U, Strouhal number St, and the cylinder diameter D, the period is calculated using the Strouhal relation ($T = D/StU$). The period is verified and measured using experimental data. Finally, owing to the reference phase and the period, other phases can be acquired by delaying the acquisition time (time shifts), which variates with the frequency of the shedding vortices. Images acquisition is performed with a commercial software (DANTEC). Non-synchronized data are recorded as well, as a baseline case, Table 1. Images are acquired through the phase-conditioning technique described earlier (microphone synchronization) for 9 different phase shifts, Table 2. Microphone synchronization indicates that the data acquisition is driven by the microphone signal (dynamic pressure signal).

3 Phases decomposition of the cylinder wake

The nearly periodic nature of the flow, due to the Von Kármán vortices, allows for the concept of phase to be defined, and, on the basis of our technique, properly assessed from data.

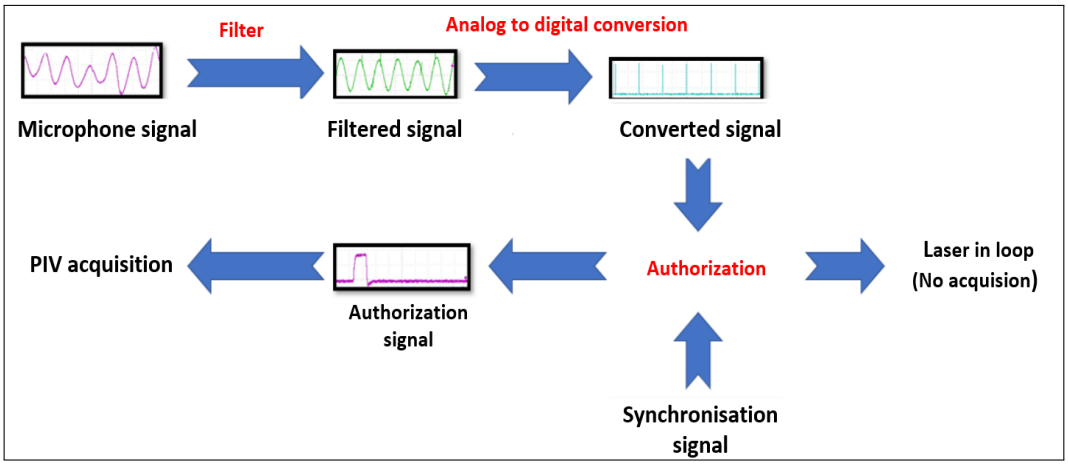

Fig. 2. Synchronization schema.

Table 1. Parameters of non-synchronized data.

Non-synchronized data				
Re number	St number	shedding freq. (*Hz*)	Phase shifts	Couple of images
2000	0.2	60	No phase shifts	10 000

Table 2. Parameters of synchronized data.

Synchronized Data				
Re number	St number	Shedding freq. (Hz)	Phase shifts	Couple of images
2000	0.2	60	9 Phase shifts each 4 ms	5000

Phase-averaged statistics (i.e., computed for each phase of the CM) may thus be appraised. The quality of phase decomposition must be first checked on lower-order statistics, such as the mean of the velocity field and Root Mean Squared. Figures 3a and 3d show the mean velocity and the RMS (Root-Mean-Squared) of the stream-wise velocity component, with no distinction among phases (without microphone synchronization). Figures 3b, 3e and Figures 3c and 3f represent the mean velocity and the RMS at $\Phi = 0°$ and $\Phi = 180°$, respectively (therefore, with microphone synchronization). Figures 3e and 3f reveal the vortex street in the wake, by figuring out the fluctuations at a particular phase of acquisitions. RMS is maximum in regions where shear is most important and gradually decreases downstream behind the obstacle. The spatial distribution of the Vortex-street patterns at $\Phi = 0°$, is typically opposed to that at $\Phi = 180°$. This emphasizes the precision of the microphone synchronization in the Particle Images Velocimetry (PIV) measurements system. The second check on the quality of phase decomposition is the triple decomposition method. It is a mathematical decomposition of turbulent fields which accounts for the quasi-periodicity of the CM, for each phase. Tracking the CM and its dynamics provides a significant insight into the nature of the flow.

$$\underbrace{f(x,t)}_{\textbf{Instantaneous}} = \underbrace{\overline{f(x,t)}}_{\textbf{Time average}} + \underbrace{f_c(x,t)}_{\textbf{Coherent motion}} + \underbrace{f_r(x,t)}_{\textbf{Random motion}}. \quad (1)$$

This equation corresponds to the decomposition first proposed by Hussein and Reynolds [10] for an organized wave, further used as a clock for selecting samples. They decomposed the instantaneous turbulent field $f(x,t)$ into three main components: time average $\overline{f(x,t)}$ (mean of the non-synchronized data), the random fluctuations in an instantaneous field $f_r(x,t)$ and the coherent structures (CM) $f_c(x,t)$ (Eq. (1)). Coherent motion (CM) is obtained by difference between the phase average $< f(x,t) >$ (mean of the synchronized data) and the time average $\overline{f(x,t)}$ (Eq. (2)).

$$\underbrace{f_c(x,t)}_{\textbf{Coherent motion}} = \underbrace{< f(x,t) >}_{\textbf{Phase average}} - \underbrace{\overline{f(x,t)}}_{\textbf{Time average}}. \quad (2)$$

The random fluctuations are found by difference between the instantaneous velocity field and the phase average (Eq. (3)),

$$\underbrace{f_r(x,t)}_{\textbf{Random motion}} = \underbrace{f(x,t)}_{\textbf{Instantaneous}} - \underbrace{< f(x,t) >}_{\textbf{Phase average}}. \quad (3)$$

Figure 4 shows the instantaneous triple decomposition of the wake, at Re = 2000 and at phase = 0°. The three components in the figure clarify one instantaneous velocity field. To check the validity of this decomposition, coherent motion is able to be realised. Coherent motion is dominant near the cylinder, but gradually weakens before disappearing as the distance from the cylinder increases, as shown in $f_c(x,t)$ of Figure 4. Coherent motion (CM) renders the flow more complex, as it induces additional shear and interactions with other scales of the motion. Coherent motion enhances the exchange of energy between different flow components. One way to detect and assess energy production and exchange mechanisms is to investigate the turbulent kinetic energy (TKE) budgets. TKE budget evidences how Coherent motion contributes to different phenomena.

4 One-point turbulent kinetic energy

We made sure that all phases of the CM are correctly extracted through the technique based on the microphone reference. Transport equation for the turbulent kinetic energy is further

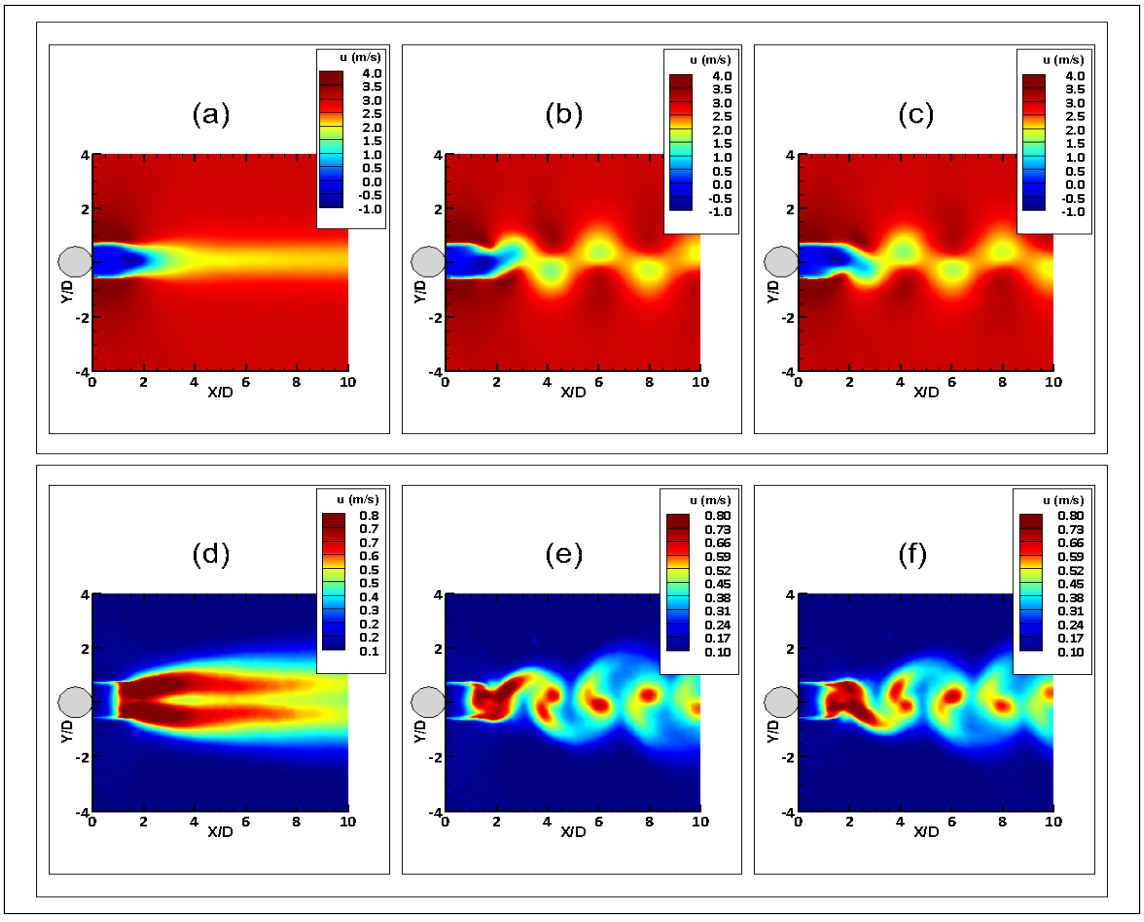

Fig. 3. (a) and (d) are the nonsynchronized mean velocity and RMS along x direction, respectively. (b) and (e) are the synchronized mean velocity and RMS along x direction at $\Phi = 0°$, respectively. (c) and (f) are the synchronized mean velocity and RMS along x direction at $\Phi = 180°$, respectively.

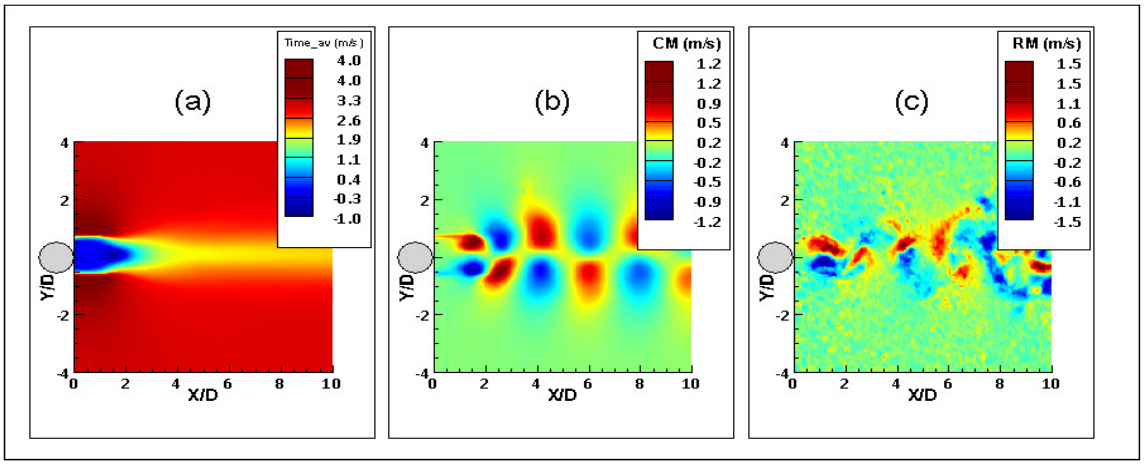

Fig. 4. Triple decomposition for Re = 2000 and $\Phi = 0°$. (a) Time average $\overline{f(x,t)}$. (b) Coherent structures (CM), $f_c(x,t)$. (c) The random fluctuations in an instantaneous field (RM), $f_r(x,t)$.

reported. This equation explains the nature and the mechanics of the turbulence in the flow at one point, (Eq. (4)). In equation (4), U and V are the mean velocities along x and y directions respectively. Terms u and v represent the fluctuations of the instantaneous velocity field along x and y direction, *respectively*. q^2 represents the kinetic energy, computed with the axisymmetry hypothesis $(2u^2+v^2)$, consequent from higher magnitude of v component compared to other components, as shown in Thiesset study [9]. Finally, ε is the kinetic energy dissipation rate. The TKE transport equation contains four main terms (Advection, Generation, Diffusion and Dissipation). The first term in the equation is the advection, or the transport of the fluctuations due to mean velocity. Advection terms along x and y directions are reported. Generation of turbulent energy is the second term, and will be greatest near the position of maximum shear and zero along the axis of symmetry. It represents the exchange of kinetic energy between the mean flow and turbulent fluctuations. In general, the energy exchange involves a loss of the mean flow and gain to the turbulence. The third term is the diffusion, which is divided into diffusion due to pressure and diffusion due to turbulence. Turbulent diffusion term explains how the turbulent kinetic energy is diffused from locations where it is produced, to other places where production is smaller, or absent. The last term is the dissipation (occurring at smallest scales, or Kolmogorov scales), and reflects the work done by smallest eddies against viscous stresses.

$$\underbrace{\left(\underbrace{U\frac{\partial(\overline{0.5q^2})}{\partial x}}_{\text{Advection on x}}+\underbrace{V\frac{\partial(\overline{0.5q^2})}{\partial y}}_{\text{Advection on y}}\right)}_{\text{Advection}}+\underbrace{\left(\overline{uv}\frac{\partial U}{\partial y}\right)}_{\text{Generation}}+\underbrace{\left(\underbrace{\frac{\partial\overline{pv}}{\partial y}}_{\text{by pressure}}+\underbrace{\frac{\partial(\overline{0.5q^2v})}{\partial y}}_{\text{by turbulence}}\right)}_{\text{Diffusion}}+\underbrace{\varepsilon}_{\text{Dissipation}}=0. \quad (4)$$

As our analysis is based upon 2D-2C PIV, terms involving derivatives are not available. For instance, it is well known that the energy dissipation rate is underestimated. Other methods are to be used to assess the correct values of this quantity. The dissipation rate is first computed by equation (5), and then corrected using Chen & Zhou [11] data to get access to the non-resolved data. The dissipation rate ε_{PIV} (computed from PIV data) is much smaller than the values of ε estimated with hot wire anemometry (Chen & Zhou [11]). Therefore, a correction is applied to ε_{PIV} to reach the values reported by Chen & Zhou [11] for the same flow, and for the same Reynolds number.

$$\varepsilon_{PIV}=\gamma\left[\frac{5}{3}\overline{\left(\frac{\partial u}{\partial x}\right)^2}+2\overline{\left(\frac{\partial u}{\partial y}\right)^2}+\overline{\left(\frac{\partial v}{\partial x}\right)^2}+\frac{8}{3}\overline{\left(\frac{\partial v}{\partial y}\right)^2}\right]. \quad (5)$$

4.1 Without phases decomposition

The leading studies of one point turbulent kinetic energy equation was accomplished by Osborne Reynolds [12], which refers to as the exchange of energy of total fluctuations (CM & RM). In this framework, each term of the equation was assessed to perceive the mechanism of turbulent kinetic energy (Generation – Transport – Dissipation). Figure 6 shows all terms in equation (4), for non-synchronized data. All terms appear to be important for the first few diameters downstream, and are symmetric with respect to the center line of the wake. The terms exhibit zero values in a region just behind the cylinder, that represents the recirculation zone. Pressure field is not available from experimental data, therefore the pressure-diffusion term cannot be estimated. Therefore, this term is calculated with the TKE equation, by difference. Diffusion through pressure is thus determined from the budget equation, by considering that all the other terms are correctly evaluated. Figures 6a and 6b show the advection along x and y directions, respectively. These terms indicate the transport of the fluctuations by the mean flow. Figures 6d and 6e depict the diffusion through turbulence and through pressure, *respectively*, which in turn indicate the transport of the fluctuations through turbulence and pressure. The two main terms, advection and diffusion appear to be complementary. The positive regions in advection terms, become negative in diffusion terms and *vice versa*. This shows the conversion from the transport of the kinetic energy of the mean velocity to the transport of the kinetic energy by the fluctuation quantities. Figure 6c shows the generation term map, revealing that the maximum takes place where the maximum gradient of the mean velocity and the maximum level of anisotropy ($\overline{v^2}/\overline{u^2}>1$ or $\overline{v^2}/\overline{u^2}<1$) occur. Figure 6f shows the dissipation term, where the maximum value is at the center line of the wake. The dissipation is maximum where higher strain and shear occur, which enhances the energy of the small scales. All terms show a good agreement with the results obtained by Thiesset [9]. Figure 5 shows profiles parallel to y direction at $X/D=2$, starting from the center line of the wake. Total advection and total diffusion have the same trace with different signs as discussed before. The dissipation is maximum at the center line of the cylinder and gradually decreases. The generation is zero at the center line and maximum in high shear regions. This is in agreement with the previous studies of Townsend [8] performed at higher Reynolds number (8400) and using hot wire anemometry.

4.2 With phase decomposition

The validation of the data non-synchronized through literature, allows us to move forward with the TKE computation of the data synchronized with the microphone. Figures 7a and 7b show advection along x and y directions, respectively, for synchronized data and for four different phases. This shows the evolution of the transport by the mean flow between the phases. Figure 7a shows at each vortex of the Von-Kármán street, positive and negative advection values follow each other, yielding a source of vorticity. Figure 7b shows high advection just behind the cylinder where the rolling-up process starts. Figures 8a and 8b show diffusion through turbulence and diffusion through pressure for different phases, respectively. As aforesaid, the kinetic energy is carried from generation regions, through the advection and diffusion processes. This is shown at $(X/D=2, Y/D=0.5)$ at any phase, for instance. Figures 9a and 9b show the generation and the dissipation terms for different phases, respectively. Figure 9a shows the vortices generation, which is associated to the onset of the Von-Kármán street. The dissipation rate is distributed over the whole flow and is not necessarily large in regions of strong generation, as shown in Figure 9b. However, the maximum dissipation is very close to the cylinder, and this increases at phase 90° and phase 270°. As previously shown in synchronized data, all terms change sign after a half period. This shows the accuracy of the phase decomposition in the wake.

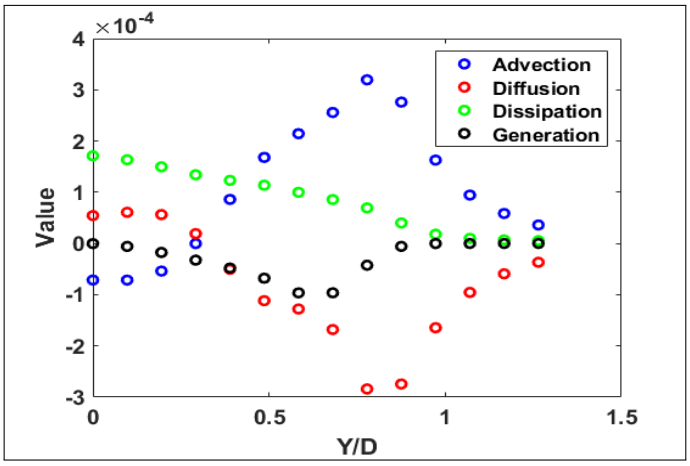

Fig. 5. TKE terms profiles for nonsynchronized data, at Re = 2000 ($X/D = 2$).

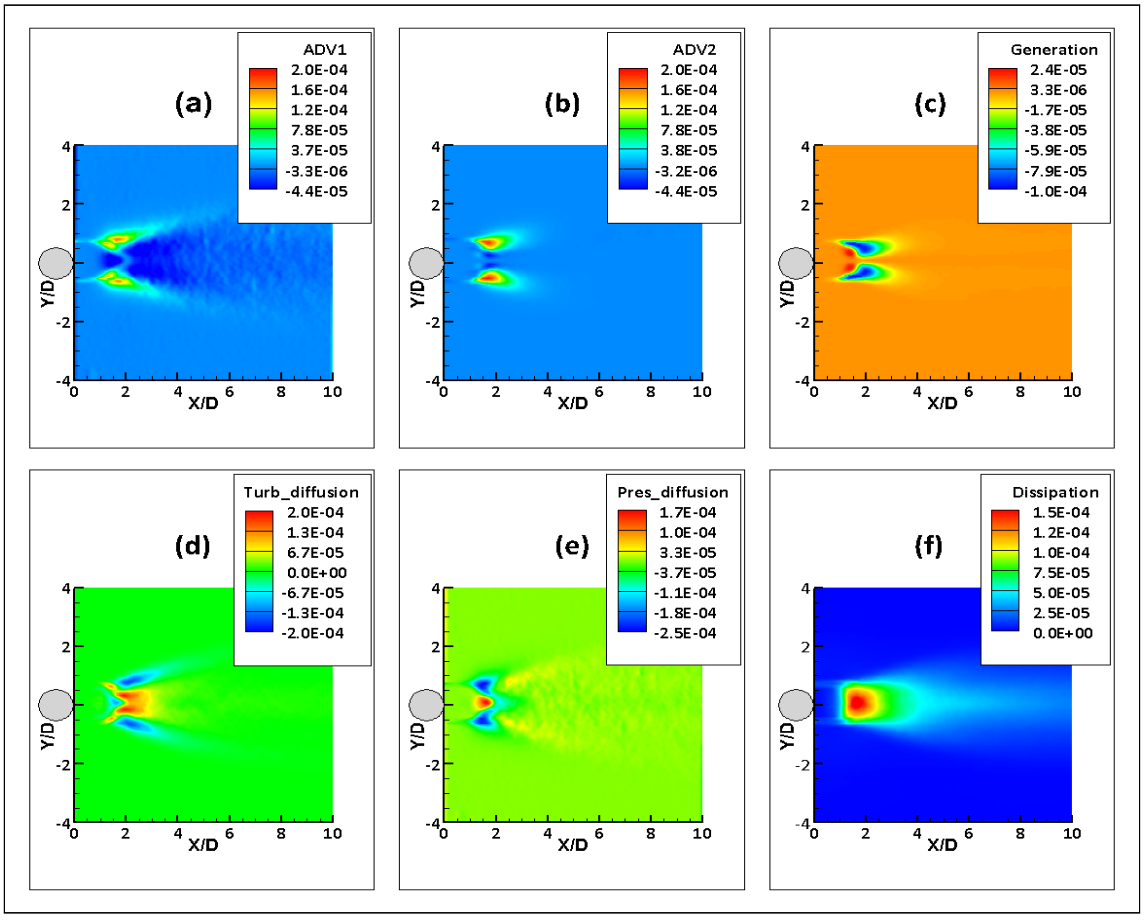

Fig. 6. One-point turbulent kinetic energy balance at Re = 2000 without microphone synchronization. All the terms are normalised by D/U_0^3. (a) Advection on x direction term $U\frac{\partial(0.5\overline{q^2})}{\partial x}$.(b) Advection on y direction term $V\frac{\partial(0.5\overline{q^2})}{\partial y}$. (c) Generation term $\overline{uv}\frac{\partial U}{\partial y}$. (d) Diffusion term through turbulence $\frac{\partial\overline{0.5q^2v}}{\partial y}$. (e) Diffusion term through pressure $\frac{\partial\overline{pv}}{\partial y}$. (f) Dissipation term ε.

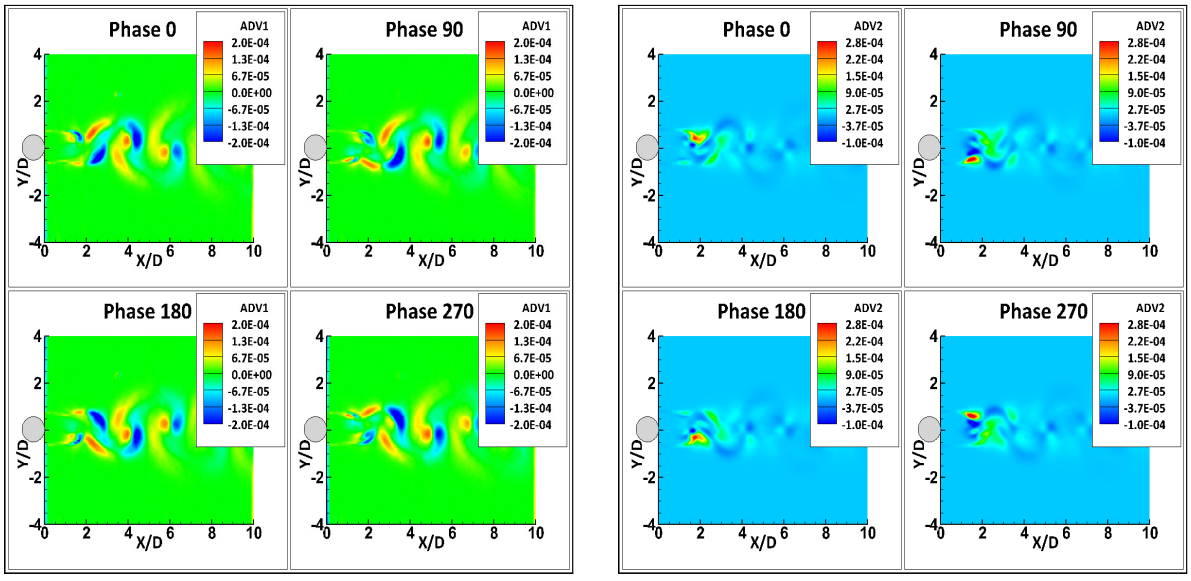

(a) *(b)*

Fig. 7. One point turbulent kinetic energy balance at Re = 2000 with microphone synchronization at 0°, 90°, 180° and 270° phase shifts. All the terms are normalised by D/U_0^3. (a) Advection on x direction term $U\frac{\partial(0.5\overline{q^2})}{\partial x}$.(b) Advection on y direction term $V\frac{\partial(0.5\overline{q^2})}{\partial y}$.

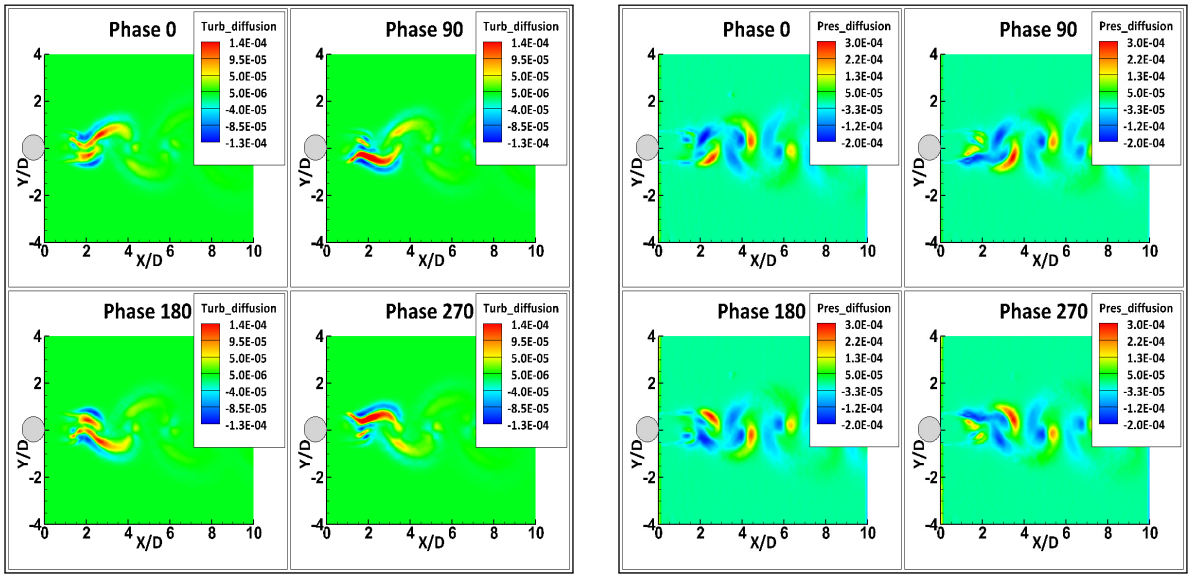

(a) *(b)*

Fig. 8. One-point turbulent kinetic energy balance at Re = 2000 with microphone synchronization at 0°, 90°, 180° and 270° phase shifts. All terms are normalised by D/U_0^3. (a) Diffusion through turbulence $\frac{\partial\overline{0.5q^2v}}{\partial y}$. (b) Diffusion through pressure $\frac{\partial\overline{pv}}{\partial y}$.

5 Two-point turbulent kinetic energy

Higher order moments are of paramount importance in the fundamental understanding of the dynamics of turbulent flows. However, the second-and-third order structure functions reflect a simpler information on the physics of the flow, as they indicate the scale-by-scale energy and the direction towards which this energy flows across scales. Equation (6) defines the second-order structure function, S_2, where the velocity (fluctuations) difference (also called increment) is measured over a spatial distance r and the average is done over x (which is interpreted as an ensemble average). Results are presented at the center-line of the cylinder wake and around 2cm downstream ($X/D = 2, Y/D = 0$). Second-order structure functions at a scale r indicate the energy contained at all scales smaller or equal to r. Equation (7) defines the third-order structure function, S_3. The sign of S_3 indicates the direction of the cascade (negative for a direct cascade, i.e. in which largest scales break

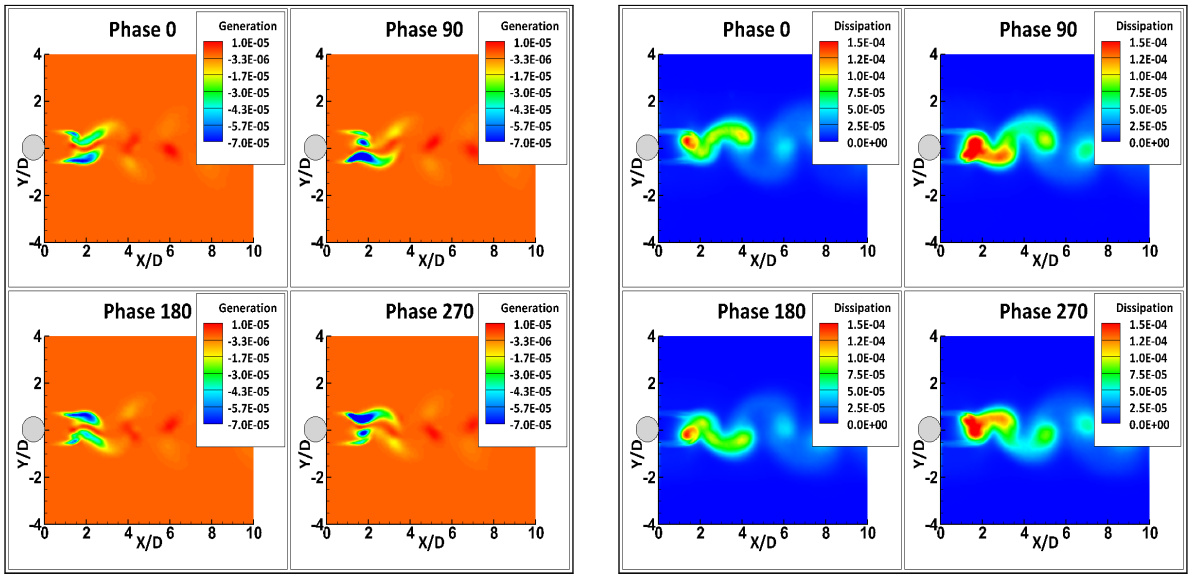

(a) *(b)*

Fig. 9. One-point turbulent kinetic energy balance at Re = 2000, with microphone synchronization at 0°, 90°, 180° and 270° phase shifts. All terms are normalised by D/U_0^3. (a) Generation term $\overline{uv}\frac{\partial U}{\partial y}$. (b) Energy dissipation rate term ε.

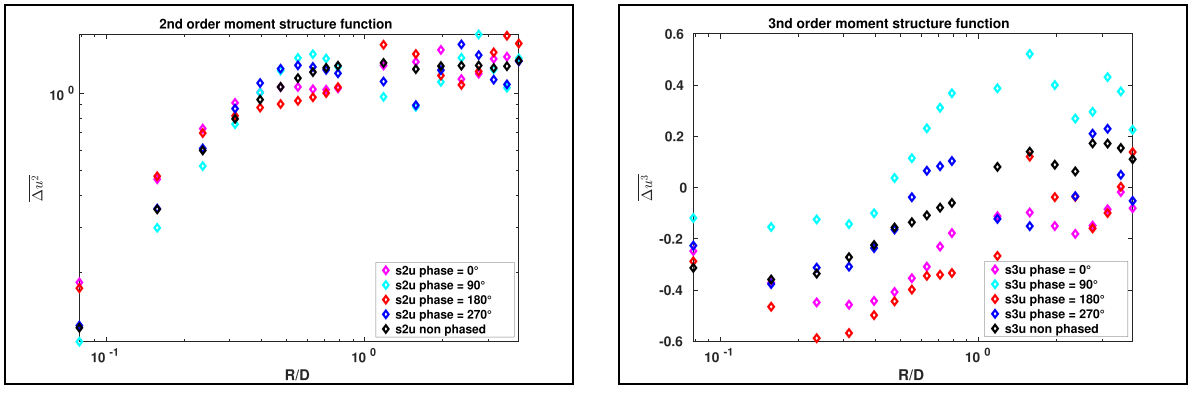

(a) *(b)*

Fig. 10. Two-point turbulent kinetic energy balance at Re = 2000, with microphone synchronization at 0°,90°,180°,270° phase shifts and without microphone synchronization.(a) 2nd order moment structure functions $(\delta u)^2$, normalised by $\overline{(\delta u)^2}$.(b) 3rd order moment structure functions $(\delta u)^3$, normalised by $(\delta u)^{3/2}$.

down and result in smaller and smaller eddies).

$$S_2 = \overline{(\delta u)^2} = \overline{(u(x+r) - u(x))^2}. \quad (6)$$

$$S_3 = \overline{(\delta u)^3} = \overline{(u(x+r) - u(x))^3}. \quad (7)$$

Figures 10a and 10b show the second and the third order structure functions (S_3 is appropriately normalized with the use of the second-order structure functions), for four different phases in addition to the baseline case (without phases decomposition), respectively. The phased data in Figure 10a highlight the energy distribution for different phases. At $r/D = 1$, the maximum energy is contained for the phase 90°, and the smallest for the opposite phase 180°, in agreement with the passage of the coherent motions. For example, the energy of large scales at phases 90° and 270° are slightly higher than the phases 0° and 180° before higher variations of the phases ($R/D = 10^0$). This can be linked to higher generation at these phases in one point TKE. However, values of S_2 for non phased data are in between results for different phases, with the same energy for large scales. For larger scales, oscillations of S_2 are visible, with periods proportional to the distance between two successive vortices in the Von Kármán street.

Third-order structure highlight a direct cascade (negative S_3) at smaller scales for all cases (with and without phase decomposition), as shown in Figure 10b. The direct cascade indicates the break-down of large scales to form smaller scales. Small scales at phases 90° and 270° have a slight lower amplitude of the cascade. This emphasizes the higher dissipation at phases 90° and 270°, as shown in one point TKE. Larger scales are

tending towards an inverse cascade, where distinctly observed at phase 90 °.

6 Conclusion

The present study is an analysis of the cylinder wake dynamics as a function of the upstream flow. Microphone sensor is installed in the flow to synchronize the data acquisition to coherent structure generation. This technique helps us to experimentally assess phase averages, with high resolution. Validation of the phase decomposition is done through the computation of turbulence statistics (mean and RMS) and through the triple decomposition method. TKE (Turbulent kinetic energy) assessments were carried out for both non-synchronized and data synchronized with microphone. TKE computations were performed for different phases to get an insight into the energy exchanges and their evolution at different phases of the flow. The distributions of different terms as a function of the phase change sign after a half period, which guarantees the correct phase decomposition of the motion in the wake. Coherent motion (CM) shows its prominence by contributing in wakes TKE exchange. The present study shows the complement between one and two point TKE exchange for a better understand of near wake cylinder.

Acknowledgement. The project (DYNEOL) was funded by the French National Research Agency (ANR) under contract no. ANR-17-CE06-0020.

References

[1] M.S. Bloor, J. Gerrard, Measurements on turbulent vortices in a cylinder wake, J. Fluid Mech. **24** (1966)
[2] A. Roshko, On the development of turbulent wakes from vortex street, National Advisory committee for aeronautics, 1954
[3] C. Williamson, Vortex dynamics in the cylinder wake, J. Fluid Mech. **28**, 477–539 (1996)
[4] M. Unal, D. Rockwell, On vortex formation from a cylinder. Part 1. The initial instability, J. Fluid Mech. **190**, 491–512 (1988)
[5] F.H. Abernathy, R.E. Krounauer, The formation of vortex streets, J. Fluid Mech. **13**, 1–20 (1961)
[6] G.S. Triantafyllou, M.S. Triantafyllou, C. Chryssostomidis, On the formation of vortex streets behind stationary cylinders, J. Fluid Mech. **170** 461–477 (1986)
[7] B. Cantwell, D. Coles, An experimental study of entrainment and transport in the turbulent near wake of a circular cylinder, J. Fluid Mech. **136**, 321–374 (1983)
[8] A. Townsend, The structure of turbulent shear flow, University of Cambridge, The Pitt building, Trumpington street, Cambridge, 1976
[9] F. Thiesset, Exploration analytique et expérimentale des interactions cohérence-turbulence au sein d'un écoulement de sillage, Université de Rouen, 2011
[10] A. Hussain, W. Reynolds, The mechanics of an organized wave in turbulent shear flow, J. Fluid Mech. **41** (1970)
[11] J. Chen, T. Zhou, Characteristics of the turbulent energy dissipation rate in a cylinder wake, J. Fluid Mech. **835**, 271–300 (2018)
[12] O. Reynolds, On the dynamical theory of incompressible viscous fluids and the determination of criterion, 1894

Cite this article as: M. Armaly, E. Varea, C. Lacour, L. Danaila, B. Lecordier, Interaction of turbulent kinetic energy and coherent motion in the near field of the cylinder wake, Mechanics & Industry **24**, 44 (2023)